Analytica Chimica Acta 1228 (2022) 340358

Contents lists available at ScienceDirect

Analytica Chimica Acta

journal homepage: www.elsevier.com/locate/aca

$In_2O_3/CdIn_2S_4$ heterojunction-based photoelectrochemical immunoassay of carcinoembryonic antigen with enzymatic biocatalytic precipitation for signal amplification

Xue Huang, Qianyun Lin, Liling Lu, Meijin Li **, Dianping Tang *

Key Laboratory for Analytical Science of Food Safety and Biology (MOE & Fujian Province), Department of Chemistry, Fuzhou University, Fuzhou, 350108, China

HIGHLIGHTS

- A photoelectrochemical immunoassay was constructed for carcinoembryonic antigen.
- $In_2O_3/CdIn_2S_4$ heterojunctions used as the photoactive materials.
- Integration of PEC with biocatalytic precipitation explored for PEC immunoassay.
- Enzyme biocatalytic precipitation utilized for the signal amplification.

GRAPHICAL ABSTRACT

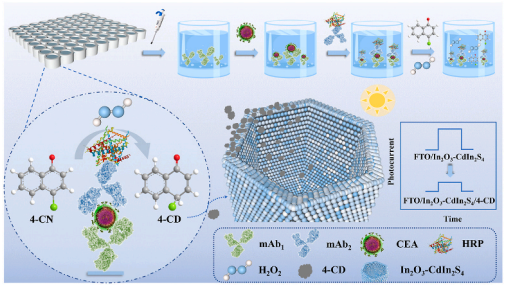

ARTICLE INFO

Keywords:
Photoelectrochemical immunoassay
$In_2O_3/CdIn_2S_4$ heterojunctions
Enzymatic biocatalytic precipitation
Carcinoembryonic antigen

ABSTRACT

This work reported a split-type photoelectrochemical (PEC) immunoassay for the detection of carcinoembryonic antigen (CEA) based on target-induced biocatalytic precipitation (BCP) by using $In_2O_3/CdIn_2S_4$ heterojunctions as the photosensitizers. The synthesized $In_2O_3/CdIn_2S_4$ heterojunctions improved the efficiency of charge separation and shortened the electron convey path to enhance the photocurrent, thus exhibiting high conductivity and low complexation rates of photogenerated electrons and holes. In the presence of CEA, horseradish peroxidase (HRP) catalyzed 4-chloro-1-naphthol (4-CN) to produce benzo-4-chloro-hexadienone (4-CD) through H_2O_2. Then, 4-CD was deposited onto the surface of $In_2O_3/CdIn_2S_4$ to reduce the photocurrent and realized the signal amplification. The PEC immunoassay revealed an excellent photocurrent toward target CEA within a wide range of 0.01–50 ng mL^{-1} at a low limit of detection of 2.8 pg mL^{-1} under the optimum conditions. Multiple switching light excitation tests demonstrated the good reliability and stability of the fabricated PEC biosensor. The accuracy was acceptable in comparison with human CEA enzyme-linked immunosorbent assay (ELISA) kit.

1. Introduction

Cancer, usually referred to the malignant tumors originating from epithelial tissue, is considered to be the most common type of diseases [1]. Cancer has become one of the most important diseases that threaten our life and health due to its low cure rate and extremely high mortality

* Corresponding author.
** Corresponding author.
E-mail addresses: mjli@fzu.edu.cn (M. Li), dianping.tang@fzu.edu.cn (D. Tang).

https://doi.org/10.1016/j.aca.2022.340358
Received 21 August 2022; Received in revised form 1 September 2022; Accepted 2 September 2022
Available online 7 September 2022

rate, especially in the middle and late stages of cancer [2]. Carcinoembryonic antigen (CEA) has been ascribed to be one of the essential tumor markers, which is usually associated with pancreatic cancer, breast cancer and lung cancer [3,4]. Persistently high levels of CEA may indicate that colorectal, breast, and lung cancers risk in humans [5], so it is often used as a sign of some tumor symptoms in clinic. Of particular note, non-smoking patients with CEA greater than 5.0 ng mL^{-1} were identified as having elevated CEA, but a smoker patient will not be considered until CEA >10 ng mL^{-1} [6]. Sensitive detection of CEA values in serum at an early stage is effective for the timely treatment of patients who may have cancer, mainly due to the fact that their survival rate can be greatly improved through early screening and clinical diagnosis of cancer [7,8]. Up to now, several strategies including colorimetry, fluorescence, electrochemiluminescence, and electrochemical methods have been developed for the detection of CEA [9,10]. Among them, photoelectrochemical (PEC) biosensor is a burgeoning technology to measure RNA, proteins, ions, micro-molecules, and other trace biological samples in recent decades [11]. It is developed from the electrochemical biological analysis technology, which separates two kinds of energy sources (light source) and detection signal (electrical signal), thus exhibiting the inherent advantages of low background, fast response and high sensitivity [12,13]. In addition, PEC bioanalytical methods are easy to be miniaturized and popularized due to the simplicity of instrumentation and operation, and have been commonly used in cancer surveillance and food safety [14–16].

The choice of appropriate photoactive materials is the imperative for the construction of PEC biosensor [17]. The AB_2C_4 (A = Cd, Cu, Zn etc.; B = In, Al, Ga etc.; C = S, Se, *etc.*) materials are known as bimetallic chalcogenides, which have attracted much attention due to the unique photoelectronic properties and adjustable band gap structure [18]. $CdIn_2S_4$, an n-type semiconductor photocatalyst with remarkable properties, has aroused wide researcher concern due to the befitting conduction band (CB) and valence band (VB) positions, superior visible-light absorption ability and the suitable band gap (~2.2 eV) [19,20]. Nevertheless, the recombination of photo-generated charge is likely to happen on the surface of the single-component $CdIn_2S_4$, as well as the little active sites and weak electron transfer, which extremely impede its use in PEC devices [21]. Several strategies had been put forward to address these issues, including defect engineering, modification of the surface, and fabrication of the heterostructures [22,23]. Generally, the construction of heterostructures is considered as one of the main proposals to address the charge and hole complex behavior in the PEC process [24,25]. For instance, Ren et al. [26] constructed a new heterojunction by the combination of $CdIn_2S_4$ and SnS_2, which can extremely promote the photocatalyst activity of hydrogen evolution due to the rapid separation of photo-generated carriers. Yu et al. [25] synthesized a novel $CdIn_2S_4/MoS_2$ composites, which showed satisfactory hydrogen production performance due to the efficient loading of MoS_2 on the surface of the $CdIn_2S_4$. Therefore, the construction of $In_2O_3/CdIn_2S_4$--based heterojunction, as a huge amount of potential and operational strategy, exhibiting high conductivity and low complexation rates of photogenerated electrons and holes.

In recent years, metal-organic frameworks (MOFs) are composed of covalent bonds between organic ligands and metal ions [27–29], which have received a lot of attention in a variety of domains, including chemical sensors, gas storage and separation, chemical catalysis and so on [30]. MIL-68 (In) as the most commonly used MOF material, which have large specific surface area and high porosity [31,32]. Sun et al. annealed MIL-68 (In) and derived In_2O_3 hollow nanotubes with porous structure [33]. This derived heterostructure retains the porous structure of MIL-68 [34]. In addition, the hollow tube structure of In_2O_3 improves light utilization by adjusting the reflection and refraction of incident light, and provides a large specific surface area and abundant active exposure sites for specific reactions [35–37]. As a representative metal oxide material, the band gap of In_2O_3 is about 2.8 eV, which has appropriate band positions as well as matched energy level with $CdIn_2S_4$ [17,22,23]. Lately, Lou et al. have synthesized two In-MOF-derived heterostructures ($ZnIn_2S_4/In_2O_3$ and $In_2S_3/CdIn_2S_4$) [38–40], which can improve CO_2 photoreduction performance due to the acceleration of separation and convey of the electron carriers. As an efficient PEC substrate, the $In_2O_3/CdIn_2S_4$ heterostructures are considered to possess the great potential to be used for signal amplification. However, there are few reports on the application of $In_2O_3/CdIn_2S_4$ heterostructures alone in the field of photoelectricity and need to be further studied.

In this work, we constructed a split-type photoelectrochemical (PEC) immunoassay for the detection of the target carcinoembryonic antigen (CEA) based on biocatalytic precipitation (BCP) by using $In_2O_3/CdIn_2S_4$ heterojunction as photoactive materials. In this design, the composite material $In_2O_3/CdIn_2S_4$ with good photoelectric activity was used as the photoactive material. The HRP enzymes catalyzed 4-CN to produce 4-CD precipitates *via* H_2O_2 [41–44] at the $In_2O_3/CdIn_2S_4$ electrode surface in the presence of the targe CEA, which significantly reduced the photocurrent. Due to the deposition of insoluble substance on the $In_2O_3/CdIn_2S_4$ electrode surface, BCP [45] amplified the signal to increase the detection limit of particular motivation to this work is the probability of integrating photoelectrochemical and biocatalytic precipitation for the exploitation of PEC immunoassays with excellent anti-interference ability and ultra-high sensitivity. Compared with the traditional enzyme reaction, the sensor exhibited excellent anti-interference ability because the solution of enzyme precipitation process was separated from the solution of PEC detection, which could be utilized for the specific detection of CEA in actual biological samples.

2. Experimental

2.1. Preparation of MOFs-derived In_2O_3

With some adjustments, a previously described oil bath process was used to create the MIL-68(In) nanorods [35]. Briefly, $In(NO_3)_3{\cdot}xH_2O$ (60 mg) and 1,4-benzenedicarboxylic acid (60 mg) were dissolved in N, N-Dimethylformamide (40 mL) under continuous stirring for 5 min to form a clear solution. Thereafter, the solution reacted in an oil bath (120 °C) for 0.5 h. The white precipitate was extracted by centrifugation after the solution had been cooled to room temperature (25 °C), washed successively with ethanol and DI water, and then dried in vacuum for a whole night at 60 °C.

Then, to obtain the hollow In_2O_3 nanotubes, the prepared MIL-68(In) prisms precursors (2.0 g) were put in a Al_2O_3 crucible and annealed at 120 °C for 2 h, removing guest molecules from pores and then dried at 500 °C for 2 h in air with a heating rate of 5 °C min^{-1}. Then the pale-yellow products were collected when the temperature was cooled.

2.2. Preparation of $In_2O_3/CdIn_2S_4$ tubular heterostructures

The $CdIn_2S_4$ nanoparticles were grown on the surface of the In_2O_3 according to a solvothermal method. Firstly, 8.0 mg of the as-obtained In_2O_3 nanotubes were dispersed in 60 mL of ethylene glycol by sonication, followed by addition of $CdIn_2S_4$ precursors (e.g., 60.2 mg of $In(NO_3)_3{\cdot}xH_2O$, 30.8 mg of $Cd(NO_3)_2{\cdot}4H_2O$, and 30.0 mg of Thioacetamide). Stirring the resulting mixture for 5 min, and then put into a Teflon-lined stainless-steel autoclave (100 mL) at 160 °C and kept for 12 h. After natural cooling, the orange-yellow products were alternately rinsed several times with ethanol and DI water, and dried in vacuum at 60 °C. The independent $CdIn_2S_4$ nanoparticles were prepared without the involvement of the In_2O_3, and other conditions were the same as described above.

2.3. Fabrication of immunoreaction PEC sensor

Scheme 1 represents a PEC sensing platform based on enzyme-catalyzed BCP for detection of the target CEA. Before the measurement, the monoclonal anti-CEA antibody (mAb_1) coated-polystyrene

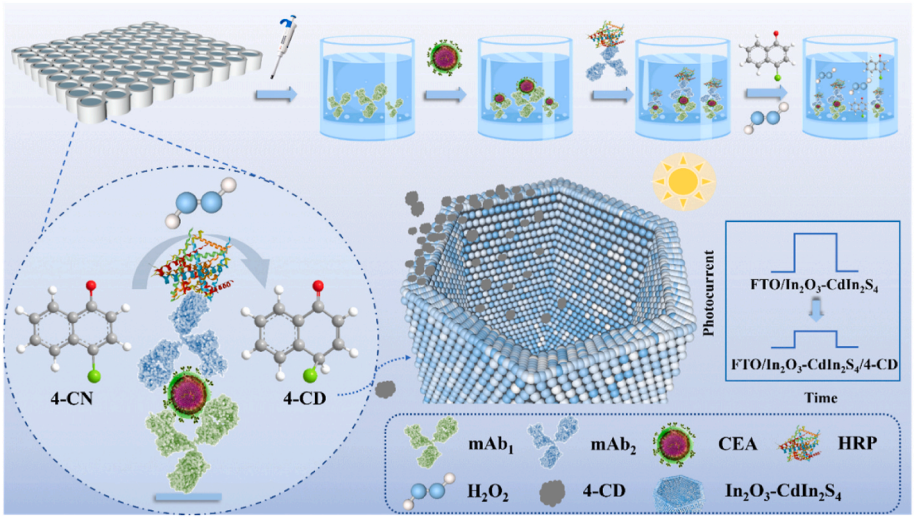

Scheme 1. Schematic diagram of PEC immunoassay for the detection of target CEA combined with HRP enzymes to catalyze the 4-CN to generate 4-CD precipitates *via* H_2O_2 for the signal amplification of $In_2O_3/CdIn_2S_4$ nanocomposites.

high-binding microplates and the HRP-labeled detection antibody (HRP-mAb_2) were prepared based on previous reports (details in supporting information). Initially, 50 μL of different concentrations of the CEA standard/sample were added to each high-binding polystyrene mAb_1-coated microplate containing PBS buffer (pH 7.0) and immunoreacted at 37 °C for 30 min, gently shaken on a rotator. To form sandwich immune structure, the preprepared HRP-mAb_2 (50 μL) with diverse concentrations was added to the above-washed microporous plates and reacted for 30 min under the same conditions. The microplates were washed in the same way as earlier. Then, 1 mM 4-CN (25 μL) and 1 mM H_2O_2 (25 μL) was added into each well and incubated at 37 °C for 40 min with slight shaking to generate 4-CD precipitates. After that, the obtained reacted solution of the microporous plates was dropped on the $In_2O_3/CdIn_2S_4$ nanocomposite-modified electrode surface at 37 °C for 10 min and dried at room temperature for subsequent measurement.

All the detection of CEA was determined in Na_2SO_4 (pH 7.4, 0.1 mol L^{-1}) solution at the applied potential of 0 V (vs. SCE) and performed on an electrochemical workstation (CHI630) with a classical three-electrode system including FTO working electrode (preprepared electrode), counter electrode (platinum electrode) and reference electrode (saturated calomel electrode). Transient photocurrents were measured at room temperature, using a 500 W xenon-lamp in the black box equipped.

3. Results and discussions

3.1. Detailed characterization MIL-68(In), In_2O_3 and In_2O_3–$CdIn_2S_4$ nanocomposites

The overall synthesis procedure of In_2O_3–$CdIn_2S_4$ hollow nanocomposites was depicted in Fig. 1A. Well-defined MIL-68(In) hexagonal were obtained by a simple solvothermal method. Next, the hexagonal In_2O_3 hollow nanotubes were synthesized through a thermal annealing method of MIL-68(In) hexagonal rods. Finally, two layers of $CdIn_2S_4$ nanoparticles were grown on the inner and outer surfaces of as-derived In_2O_3 nanotubes through the hydrothermal treatment.

The microstructure and specific morphology of the prepared materials [MIL-68(In), In_2O_3, and $In_2O_3/CdIn_2S_4$] were identified by scanning electron microscope (SEM). From the SEM image depicted in Fig. 1B and C, the bare MIL-68(In) powders exhibited a regular smooth hexagonal nanorods structure. After being annealed at high temperature, the well-aligned clavate MIL-68(In) precursor was converted into

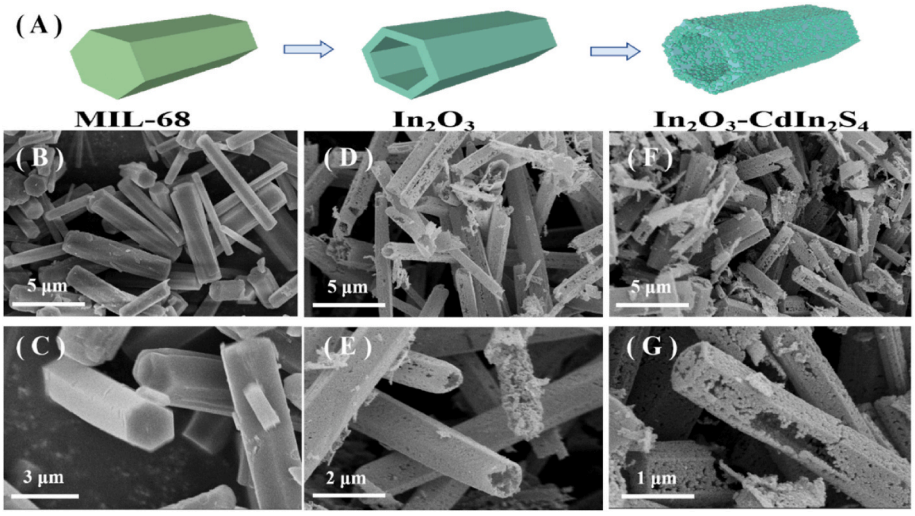

Fig. 1. (A) Fabrication procedure of the hollow $In_2O_3/CdIn_2S_4$ nanocomposites, SEM image of (B,C) MIL-68(In), (D,E) pure In_2O_3, and (F,G) $In_2O_3/CdIn_2S_4$ nanocomposites.

the In_2O_3 nanotubes retaining a rod morphology similar with the precursor (Fig. 1D and E). Nevertheless, it could be obviously observed that the hollow tube structure and a mass of voids and cracks existed on the unevenness of the surface. In addition, the size of In_2O_3 nanotubes was mildly decreased. The SEM images of $In_2O_3/CdIn_2S_4$ composite revealed that the $CdIn_2S_4$ shell and the In_2O_3 core successfully establishes the core-shell nanotubes, indicating that the aggregated $CdIn_2S_4$ nanoparticles obtained uniformly distributed over the inside and outside surface of In_2O_3 nanotubes (Fig. 1F and G). In conclusion, the evolution of the hybridized heterostructure and the successful synthesis of the final morphology were confirmed by SEM in terms of morphology.

Moreover, the crystal structure of above complexes was analyzed by X-ray diffraction (XRD), as depicted in Fig. 2A. The MIL-68(In) precursor showed several diffraction peaks at 14.1, 16.2, 16.9, 18.7, 26.3, 29.7, and 31.1°, which was consistent with previous reports [34]. The main diffraction peaks of In_2O_3 powder at 21.4, 30.5, 35.5, 51.0, and 60.6° were agree with the cubic In_2O_3 phase [(211), (222), (400), (411) (332), (440), (611) and (622)] [42], respectively, without impurities. For In_2O_3–$CdIn_2S_4$, all characteristic peaks could be found in cubic $CdIn_2S_4$ and In_2O_3, and no extra peaks appeared, suggesting that $In_2O_3/CdIn_2S_4$ with a highly hollow structure was successfully compounded.

To further verify the successful bonding of heterostructures at the elemental level and surface states, X-ray photoelectron spectroscopy (XPS) was employed to identify the configuration as well as the chemical state of In_2O_3 and $In_2O_3/CdIn_2S_4$ composites. As shown in Fig. 2B the full XPS spectrum demonstrated that C, O, and In elements were existed in In_2O_3, and C, O, Cd, In, and S elements were found in $In_2O_3/CdIn_2S_4$, which was accordant with the expected results. Fig. 2C–F reveals the high-resolution spectrum of In 3d, O 1s, Cd 3d and S 2p, respectively. After deconvolution of the In refine-spectrum, two peaks at 443.8 eV and 451.3 eV were respectively assigned to the In $3d_{5/2}$ and $3d_{3/2}$ of the pristine In_2O_3, which is consistent with the previous report [22]. It was worth noting that the $In_2O_3/CdIn_2S_4$ composites appeared two In 3d peaks at the binding energies of 444.6 eV and 452.0 eV, which were marginally shifted by 0.8 eV and 0.7 eV respectively. The binding energy shift of In 3d XPS peaks were due to the significant interaction between $CdIn_2S_4$ and In_2O_3, which were beneficial to ameliorate the charge transfer. The O 1s peaks of In_2O_3 could be deconvoluted into three peaks, including adsorbed water (O_{abs}) at 532.6 eV, surface hydroxyls (O–H) at 531.1 eV and lattice oxygen (O_L) at 529.3 eV (Fig. 2D). The binding energy of O 1s spectra for $In_2O_3/CdIn_2S_4$ shift 0.1–0.2 eV than that of In_2O_3, which might be owing to the usage of the ethylene glycol reducing agent and result that more oxygen vacancies are produced in $In_2O_3/CdIn_2S_4$ [36]. In $In_2O_3/CdIn_2S_4$ composites, the Cd $3d_{5/2}$ peak at 404.8 eV and Cd $3d_{5/3}$ peak at 411.5 eV were attributed to Cd^{2+} species [22]. As for S 2p spectrum, two peaks at 162.4 and 161.1 eV belong to S $2p_{1/2}$ and S $2p_{3/2}$, well conform to the value for S^{2-} (Fig. 2F). On the basis of the description results above collectively, it could be inferred that the $In_2O_3/CdIn_2S_4$ composite was successfully compounded.

3.2. PEC characterization of $In_2O_3/CdIn_2S_4$-modified electrode

Another additional validation required is the (photo)electrochemistry of the composite electrodes, which was closely related to the efficiency of the built PEC sensors. Electrochemical impedance spectroscopy (EIS) was intended to depict the interface characteristic of the constructed electrodes. As a rule, a larger arcradius in EIS Nyquist plots means a stronger resistance for electron transfer [46]. Fig. 3A reveals the EIS results of the $In_2O_3/CdIn_2S_4$ heterojunction, in which the semicircle of $In_2O_3/CdIn_2S_4$ was smaller than that of the MIL-68(In) and In_2O_3, suggesting that the amelioration in electron convey due to the $CdIn_2S_4$ doping. Subsequently, to further verify the amelioration in electron convey by the transient photocurrent responses of compounds. We measured the photocurrents of diverse modifying electrodes, which the MIL-68(In) modified electrode had almost no current responses and the In_2O_3 derived from the precursors, remaining a faint photocurrent as before (Fig. 3B). Consistent with expectations, after doping, the $In_2O_3/CdIn_2S_4$ possessed a stronger photocurrent response than the pure In_2O_3, correlated with its highest charge separation efficiency and shortest electron convey path. In summary, the results of EIS and transient photocurrent response indicated that the formation of the hollow tubular $In_2O_3/CdIn_2S_4$ heterostructures is the leading reason for promoting the photocatalytic activity as well as the transport and separation of the photoelectron, which could be utilized for the further successful fabrication of PEC immunoassay.

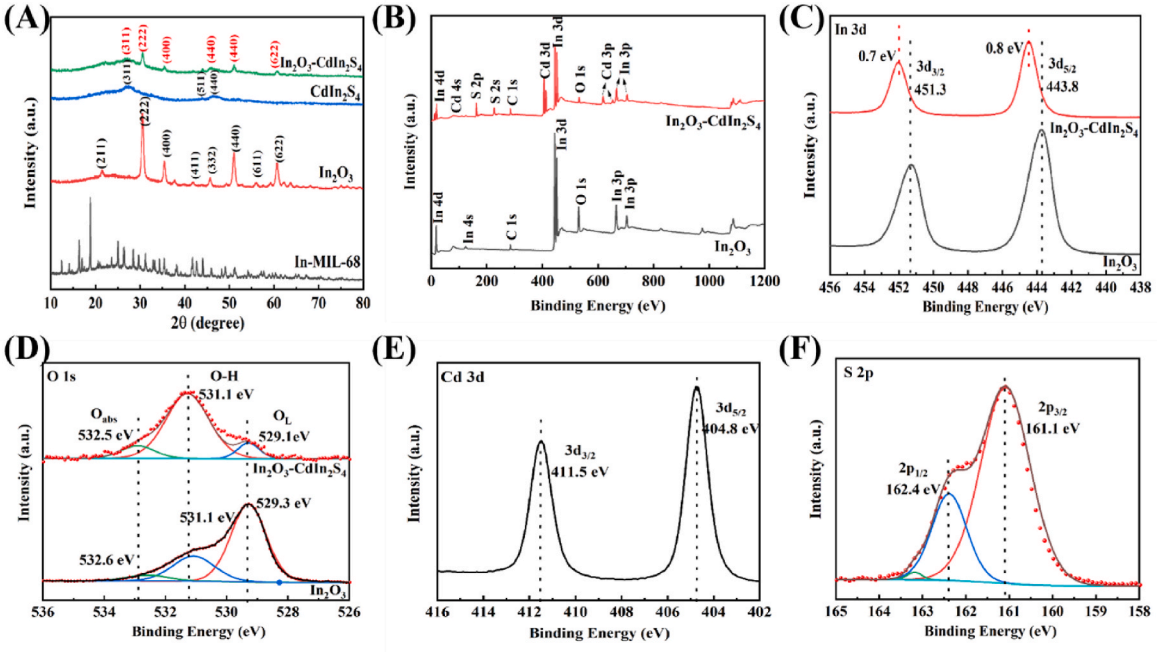

Fig. 2. (A) XRD patterns and (B) XPS survey spectrum of pure In_2O_3 and $In_2O_3/CdIn_2S_4$ nanocomposites; high-resolution XPS spectra of (C) In 3d, (D) O 1s, (E) Cd 3d and (F) S 2p.

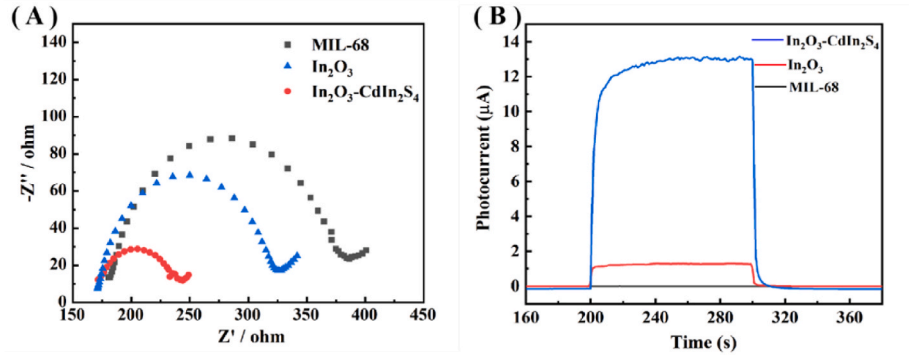

Fig. 3. (A) EIS Nyquist plots and (B) photocurrent responses of MIL-68(In), pure In_2O_3 and $In_2O_3/CdIn_2S_4$ nanocomposites.

3.3. Optimization of $In_2O_3/CdIn_2S_4$ constructed PEC immunoassay

To accomplish the preferable analysis performance of the $In_2O_3/CdIn_2S_4$ constructed PEC immunoassay, except experiment conditions such as the pH, time of the antigen-antibody incubation reaction and the incubation time of 4-CD precipitates should be investigated. As depicted in Fig. 4A, the currents increased with the enhancement of the pH values and then decreased, thus we determined that the optimal pH concentration of PBS buffer was 7.0 for subsequent detection. Then we optimized the common immunoreaction time of mAb_1 with the CEA and the mAb_1-CEA with HRP-mAb_2 taking 5 ng mL^{-1}(CEA critical values in actual human serum) as an example. Fig. 4B represents that the currents decreased with the enhancement of the immunoreaction time and then tended to be a plateau after 30 min, which could be chosen to be the best incubation time for further experiments. Finally, we explored the effect of the deposition time between 4-CD precipitates and $In_2O_3/CdIn_2S_4$ electrodes on current intensity, using 5 ng mL^{-1} CEA as an example as ever. Fig. 5C demonstrated that the deposition time of 4 min was the optimal option. Thus, we selected PBS buffer solution with pH concentration of 7.0, the incubation time of 30 min and the deposition time of 4 min as the optimal conditions.

3.4. Performance of $In_2O_3/CdIn_2S_4$ constructed PEC immunoassay

To further study the performance of the enzyme-catalyzed substrate precipitation-based PEC immunoassay, the sensor was applied to accomplish detection of CEA standards under the optimum test conditions at different concentrations. Fig. 5A revealed that with the increment of HRP concentration, more 4-CN precipitates were catalyzed, and then leading to the photocurrent of the $In_2O_3/CdIn_2S_4$ decreased by degrees. Fig. 5B displayed a preferable linear relation between the changes of current values and the logarithm of increasing CEA concentration within the actional range from 0.01 ng mL^{-1} to 50 ng mL^{-1}. The acquired regression equation was I (μA) = 2.707–5.290 × log ($C_{[CEA]}$/mg mL^{-1}) (R^2 = 0.9790, n = 8) and the detection limitation was inferred to be 2.8 pg mL^{-1} (S/N = 3).

3.5. Stability and specificity of $In_2O_3/CdIn_2S_4$ constructed PEC immunoassay

As an emerging experiment, stability and specificity were two considerable factors of the $In_2O_3/CdIn_2S_4$ constructed PEC immunoassay to detect the practical samples. Fig. 5C illustrated that the photocurrent of $In_2O_3/CdIn_2S_4$ was reproducible under 10 on/off irradiation cycles for 210 s, an indication that the excellent photostability of the PEC immunoassay. Furthermore, the $In_2O_3/CdIn_2S_4$ composites modifying electrodes were stored at 4 °C for 15, 30 and 60 days, and 98.2%, 97.6%, 95.8% (n = 3) of the initial photocurrent intensity was maintained, respectively, indicating the satisfactory storage stability of the immunoassay.

To assess the specificity of our PEC immunoassay, some representative biomarkers including prostate-specific antigen (PSA), alpha-fetoprotein (AFP) and immunoglobulin G (IgG) would serve as interfering materials with the detection accuracy of the target CEA. Fig. 5D demonstrated that the photocurrent intensity of the mixture did not change remarkably compared with the pure CEA, and the current intensity of the high concentration biomarkers was as much as the background photocurrent respectively, indicating that the presence of these biomarkers had no interference with the detection which revealed that the immunoassay possess an excellent anti-interference and outstanding specificity ability.

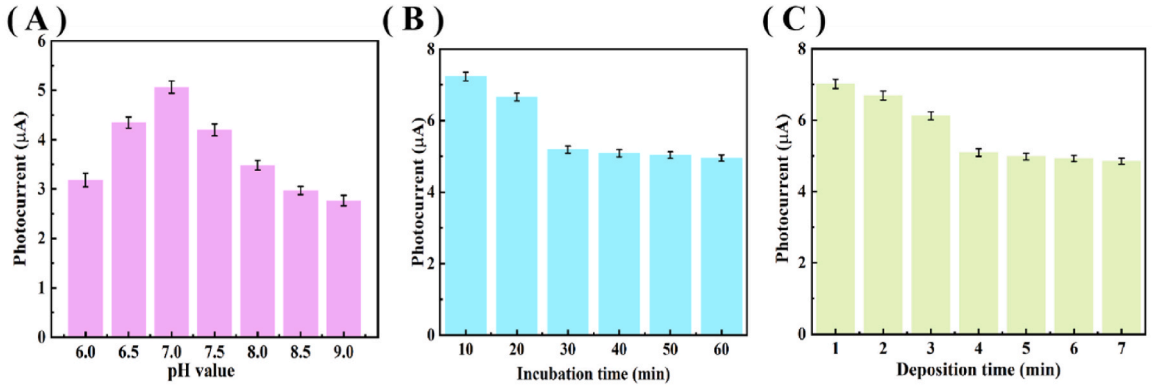

Fig. 4. Optimization of (A) pH value of PBS buffer solution, (B) incubation time of the antigen-antibody and (C) deposition time between 4-CD precipitates and $In_2O_3/CdIn_2S_4$ electrodes.

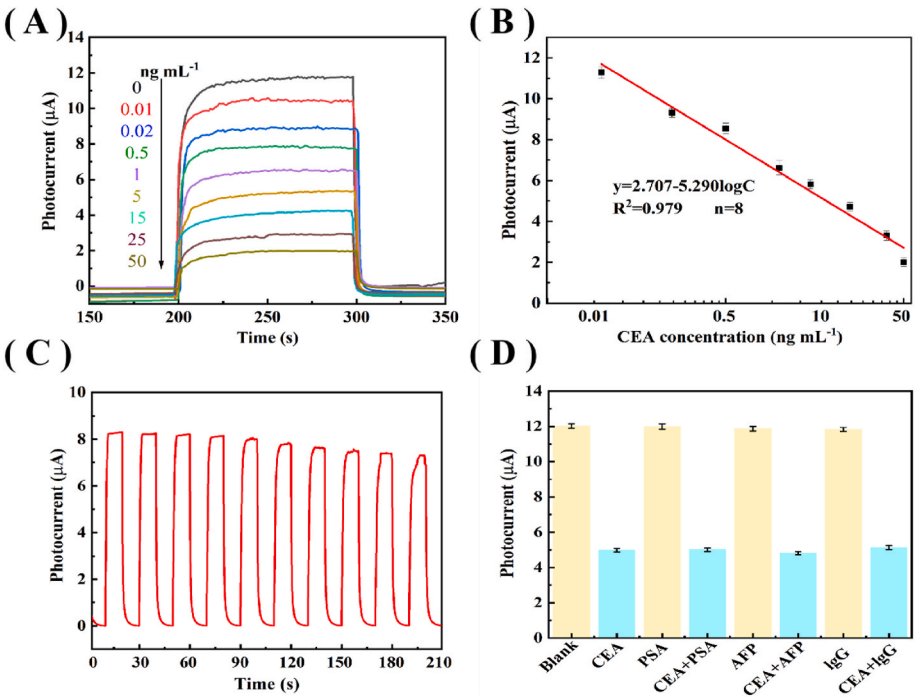

Fig. 5. (A) Photocurrent responses of PEC immunoassay in buffer PBS buffer (pH 7.0) detection of CEA standards at various concentrations; (B) Calibration curve (0.01–50 ng mL^{-1}); (C) Stability of the In_2O_3–$CdIn_2S_4$ complexes electrode; (D) Specificity of the PEC immunoassay for CEA detection: CEA: 5.0 ng mL^{-1}; PSA: 80 ng mL^{-1}; AFP: 80 ng mL^{-1}; IgG: 80 ng mL^{-1}.

3.6. Analysis of human serum samples

To examine the practicality as well as the accuracy of our proposed PEC immunoassay in real human samples, we gathered six human serum samples from Fujian Provincial Hospital (Fuzhou, China) in accordance with the Guidelines and the ethics committee of Fuzhou University. These serum samples were centrifuged for 5.0 min at 5,000*g* to remove the possible precipitation, and then determined by the developed PEC immunoassay. The obtained results were compared with those assayed by a human CEA ELISA kit. As displayed in Table 1, there was no remarkable difference between the proposed PEC test method and the commercially available CEA ELISA kits, and all calculated t_{exp} values were under 2.77 ($t_{crit[0.05,4]} = 2.77$), revealing that the proposed PEC biosensor based on BCP strategy exhibited good accuracy and stability Therefore, the proposed PEC immunoassay possessed acceptable accuracy and could be used to the early diagnostics of some cancers.

Table 1
Comparison of analytical results between PEC immunoassay and CEA ELISA kit for real samples.

Sample no.	Methods (mean ± SD, ng mL^{-1}, $n = 3$)		t_{exp}
	PEC immunoassay	CEA ELISA kit	
1	18.62 ± 1.28	17.38 ± 1.12	1.08
2	7.52 ± 0.42	7.36 ± 0.38	0.72
3	2.68 ± 0.12	2.66 ± 0.09	0.21
4	11.56 ± 0.65	11.48 ± 0.62	0.88
5	0.79 ± 0.05	0.84 ± 0.04	0.18
6	5.96 ± 0.45	6.02 ± 0.48	1.23

4. Conclusions

In conclusion, our work successfully combined biocatalytic precipitation with PEC sensing strategy to construct an $In_2O_3/CdIn_2S_4$ heterojunction based on enzyme-catalyzed substrate precipitation for detection of target CEA. Compared to the conventional PEC strategies, two remarkable advantages obtained by our experiment should be highlighted. On the one hand, the $CdIn_2S_4$ nanoparticles exhibited befitting CB and VB positions, superior visible-light absorption ability and suitable band gap. After growing on the surface of the In_2O_3, the synthesis of $In_2O_3/CdIn_2S_4$ composites could improve the efficiency of electron separation and shorten electron convey path to enhance photocurrent signal. On the other hand, the 4-CD precipitations were shifted to PEC detection cell to deposit on the surface of $In_2O_3/CdIn_2S_4$ electrodes and decreased the photocurrent signal to realize the signal amplification. More importantly, the PEC immunoassay possessed excellent stability and selectivity as well as wide linear range and low limit of the detection of CEA. Therefore, our work demonstrates the enormous potential application to exploit a convenient and low-cost strategy for early diagnostics of cancers.

CRediT authorship contribution statement

Xue Huang: Conceptualization, Methodology, Writing – original draft. **Qianyun Lin:** Visualization, Data curation, Writing – review & editing. **Liling Lu:** Visualization, Investigation, Writing – review & editing. **Meijin Li:** Visualization, Data Collection, Writing – original draft. **Dianping Tang:** Methodology, Visualization, Supervision, Funding acquisition, Project administration.

Declaration of competing interest

The authors declare that they have no known competing financial interests or personal relationships that could have appeared to influence the work reported in this paper.

Data availability

Data will be made available on request.

Acknowledgments

Authors acknowledge financial support from the National Natural Science Foundation of China (21874022 & 21675029).

Appendix A. Supplementary data

Supplementary data to this article can be found online at https://doi.org/10.1016/j.aca.2022.340358.

References

[1] H. Liang, Y. Luo, Y. Li, Y. Song, L. Wang, An immunosensor using electroactive COF as signal probe for electrochemical detection of carcinoembryonic antigen, Anal. Chem. 94 (2022) 5352–5358.
[2] L. Ding, S. Xu, Y. Huang, Y. Yao, Y. Wang, L. Chen, Y. Zeng, L. Li, Z. Lin, L. Guo, Surface-enhanced electrochemiluminescence imaging for multiplexed immunoassays of cancer markers in exhaled breath condensates, Anal. Chem. 94 (2022) 7492–7499.
[3] L. Huang, Y. Zeng, X. Liu, D. Tang, Pressure-based immunoassays with versatile electronic sensors for carcinoembryonic antigen detection, ACS Appl. Mater. Interfaces 13 (2021) 46440–46450.
[4] M. Khan, H. Ameer, Y. Chi, Label-free and ultrasensitive electrochemiluminescent immunosensor based on novel luminophores of $Ce_2Sn_2O_7$ nanocubes, Anal. Chem. 93 (2021) 3618–3625.
[5] X. Gao, J. Boryczka, S. Kasani, N. Wu, Enabling direct protein detection in a drop of whole blood with an "on-strip" plasma separation unit in a paper-based lateral flow strip, Anal. Chem. 93 (2021) 1326–1332.
[6] K. Zhang, S. Lv, Q. Zhou, D. Tang, CoOOH nanosheets-coated g-C_3N_4/$CuInS_2$ nanohybrids for photoelectrochemical biosensor of carcinoembryonic antigen coupling hybridization chain reaction with etching reaction, Sens. Actuators, B 307 (2020), 127631.
[7] F. Mo, M. Han, X. Weng, Y. Zhang, J. Li, H. Li, Magnetic-assisted methylene blue-intercalated amplified dsDNA for polarity-switching-mode photoelectrochemical aptasensing, Anal. Chem. 93 (2021) 1764–1770.
[8] Z. Qiu, J. Shu, D. Tang, Bioresponsive release system for visual fluorescence detection of carcinoembryonic antigen from mesoporous silica nanocontainers mediated optical color on quantum dot-enzyme-impregnated paper, Anal. Chem. 89 (2017) 5152–5160.
[9] Z. Yu, H. Gong, Y. Li, J. Xu, J. Zhang, Y. Zeng, X. Liu, D. Tang, Chemiluminescence-derived self-powered photoelectrochemical immunoassay for detecting low-abundance disease-related protein, Anal. Chem. 93 (2021) 13389–13397.
[10] Z. Yu, H. Gong, J. Xu, Y. Li, Y. Zeng, X. Liu, D. Tang, Exploiting photoelectric activities and piezoelectric properties of $NaNbO_3$ semiconductors for point-of-care immunoassay, Anal. Chem. 94 (2022) 3418–3426.
[11] J. Li, L. Xu, Y. Shen, L. Guo, H. Yin, X. Fang, Z. Yang, Q. Xu, H. Li, Superparamagnetic nanostructures for split-type and competitive-mode photoelectrochemical aptasensing, Anal. Chem. 92 (2020) 8607–8613.
[12] R. Xu, K. Xu, Y. Du, J. Li, X. Ren, H. Ma, D. Wu, Y. Li, Q. Wei, Dual direct Z-scheme heterojunction with growing photoactive property for sensitive photoelectrochemical and colorimetric bioanalysis, Anal. Chem. 94 (2022) 9888–9893.
[13] K. Dashtian, S. Hajati, M. Ghaedi, Molecular imprinted poly(2,5-benzimidazole)-modified VO_2-$CuWO_4$ homotype heterojunction for photoelectrochemical dopamine sensing, Anal. Chem. 94 (2022) 6781–6790.
[14] Y. Gao, Y. Zeng, X. Liu, D. Tang, Liposome-mediated in situ formation of type-I heterojunction for amplified photoelectrochemical immunoassay, Anal. Chem. 94 (2022) 4859–4865.
[15] Q. Cai, T. Yin, Y. Ye, G. Jie, H. Zhou, Versatile photoelectrochemical biosensing for Hg^{2+} and aflatoxin B1 based on enhanced photocurrent of $AgInS_2$ quantum dot-DNA nanowires sensitizing NPC-ZnO nanopolyhedra, Anal. Chem. 94 (2022) 5814–5822.
[16] Y. Gao, X. Fan, X. Zhang, Q. Guan, Y. Xing, W. Song, Switchable multiplex photoelectrochemical immunoassay of Abeta42 and Abeta40 based on a pH-responsive i-motif probe and pyrene-based MOF photocathode, Anal. Chem. 94 (2022) 6621–6627.
[17] T. Wu, J. Feng, S. Zhang, L. Liu, X. Ren, D. Fan, X. Kuang, X. Sun, Q. Wei, H. Ju, A self-powered photoanode-supported photoelectrochemical immunosensor for CYFRA 21-1 detection based on In_2O_3/In_2S_3/$CdIn_2S_4$ heterojunction, Biosens. Bioelectron. 169 (2020), 112580.
[18] Y. Li, L. Li, X. Dong, Z. Xin, J. Guan, X. Gao, W. Zu, W. Zhang, Minimalist preparation and photocatalysis properties of a spinyball-like indium-based composite suitable for different light conditions, J. Alloys Compd. 909 (2022), 164701.
[19] H. Wang, Y. Xia, H. Li, X. Wang, Y. Yu, X. Jiao, D. Chen, Highly active deficient ternary sulfide photoanode for photoelectrochemical water splitting, Nat. Commun. 11 (2020) 3078.
[20] Q. Wang, L. Wang, Y. Jiang, Y. Liu, W. Zhang, J. Zhang, A. Macauley, Morphology-engineered carbon quantum dots embedded on octahedral $CdIn_2S_4$ for enhanced photocatalytic activity towards pollutant degradation and hydrogen evolution, Environ. Res. 209 (2022), 112800.
[21] Y. Yang, Z. Chen, C. Feng, J. Jing, The $CdIn_2S_4$/WO_3 nanosheet composite has a significantly enhanced photoelectrochemical cathodic protection performance and excellent electron storage capability, Chem. Eur J. 27 (2021) 11589–11599.
[22] S. Zhao, K. Li, J. Wu, J. Zhang, X. Li, X. Guo, C. Song, Metal-organic framework-derived tubular In_2O_3-C/$CdIn_2S_4$ heterojunction for efficient solar-driven CO_2 conversion, ACS Appl. Mater. Interfaces 14 (2022) 20375–20384.
[23] D. Ma, J. Shi, Y. Zou, Z. Fan, J. Shi, L. Cheng, D. Sun, Z. Wang, C. Niu, Multiple carrier-transfer pathways in a flower-like In_2S_3/$CdIn_2S_4$/In_2O_3 ternary heterostructure for enhanced photocatalytic hydrogen production, Nanoscale 10 (2018) 7860–7870.
[24] X. Zhao, Y. Zhou, Q. Liang, M. Zhou, Z. Li, S. Xu, Coupling MOF-derived titanium oxide with $CdIn_2S_4$ formed 2D/3D core–shell heterojunctions with enhanced photocatalytic performance, Separ. Purif. Technol. 279 (2021), 119765.
[25] M. Yu, Q. Hu, X. Gong, H. Yu, S. Wang, Z. Li, Y. Chen, S. Li, The construction of three-dimensional $CdIn_2S_4$/MoS_2 composite materials for efficient hydrogen production, J. Alloys Compd. 892 (2022), 162168.
[26] T. Ren, Y. Liu, S. Yu, Synthesis of core–shell SnS_2/$CdIn_2S_4$ heterojunction photocatalyst for visible light driven hydrogen evolution, Mater. Lett. 304 (2021), 130611.
[27] H. Ding, Y. Feng, Y. Xu, X. Xue, R. Feng, T. Yan, L. Yan, Q. Wei, Self-powered photoelectrochemical aptasensor based on MIL-68(In) derived In_2O_3 hollow nanotubes and Ag doped $ZnIn_2S_4$ quantum dots for oxytetracycline detection, Talanta 240 (2022), 123153.
[28] Z. Cai, J. Dai, W. Li, K.B. Tan, Z. Huang, G. Zhan, J. Huang, Q. Li, Pd supported on MIL-68(In)-derived In_2O_3 nanotubes as superior catalysts to boost CO_2 hydrogenation to methanol, ACS Catal. 10 (2020) 13275–13289.
[29] R. Liang, Z. He, Y. Lu, G. Yan, L. Wu, High-efficiency sandwich-like hierarchical AgBr-Ag@MIL-68(Fe) photocatalysts: step-scheme photocatalytic mechanism for enhanced photoactivity, Separ. Purif. Technol. 277 (2021), 119442.
[30] P. Yong, S. Wang, X. Zhang, H. Pan, S. Shen, MOFs-derived Co-doped In_2O_3 hollow hexagonal cylinder for selective detection of ethanol, Chem. Phys. Lett. 795 (2022), 139517.
[31] D. Arif, Z. Hussain, A. Abbasi, M. Sohail, Ag functionalized In_2O_3 derived from MIL-68(In) as an efficient electrochemical glucose sensor, Front. Chem. 10 (2022), 906031.
[32] L. Wang, Y. Zhou, Q. Xu, X. Wu, G.-D. Xu, J. Guo, D. Fang, Fabrication of In_2S_3/MIL-68(In) heterojunction composite photocatalysts for degradation of Rhodamine B and hydrogen evolution, J. Porous, Mater 29 (2021) 181–192.
[33] J. Zhao, M. Zheng, X. Lai, H. Lu, N. Li, Z. Ling, J. Cao, Preparation of mesoporous In_2O_3 nanorods via a hydrothermal-annealing method and their gas sensing properties, Mater. Lett. 75 (2012) 126–129.
[34] J. Li, L. Liu, Q. Liang, M. Zhou, C. Yao, S. Xu, Z. Li, Core-shell ZIF-8@MIL-68(In) derived ZnO nanoparticles-embedded In_2O_3 hollow tubular with oxygen vacancy for photocatalytic degradation of antibiotic pollutant, J. Hazard Mater. 414 (2021), 125395.
[35] J. Wang, F. Zhang, Y. Wang, G. Luo, Preparation of $In(OH)_3$ and In_2O_3 nanorods through a novel hydrothermal method and the effect of Sn dopant on crystal structures, Ind. Eng. Chem. Res. 57 (2018) 2882–2889.
[36] Q. Wang, Y. Chen, X. Liu, L. Li, L. Du, G. Tian, Sulfur doped In_2O_3-CeO_2 hollow hexagonal prisms with carbon coating for efficient photocatalytic CO_2 reduction, Chem. Eng. J. 421 (2021), 129968.
[37] L. Jin, Q. Liu, W. Sun, Size-controlled indium(iii)–benzenedicarboxylate hexagonal rods and their transformation to In_2O_3 hollow structures, CrystEngComm 15 (2013) 4779–4784.
[38] J. Ren, K. Yuan, K. Wu, L. Zhou, Y. Zhang, A robust CdS/In_2O_3 hierarchical heterostructure derived from a metal–organic framework for efficient visible-light photocatalytic hydrogen production, Inorg. Chem. Front. 6 (2019) 366–375.
[39] T. Yan, Y. Feng, X. Ren, J. Li, Y. Lu, M. Sun, L. Yan, Q. Wei, H. Ju, Fabrication of CDs hybrid MIL-68(In) derived In_2O_3-In_2S_3 hollow tubular heterojunction and their exceptional self-powered PEC aptasensing properties for ampicillin detecting, J. Materiomics. 7 (2021) 721–727.
[40] S. Wang, B. Guan, X. Lou, Construction of $ZnIn_2S_4$-In_2O_3 hierarchical tubular heterostructures for efficient CO_2 photoreduction, J. Am. Chem. Soc. 140 (2018) 5037–5040.
[41] W. Zhao, P. Yu, J. Xu, H. Chen, Ultrasensitive photoelectrochemical biosensing based on biocatalytic deposition, Electrochem. Commun. 13 (2011) 495–497.
[42] R. Zeng, H. Gong, Y. Li, Y. Li, W. Lin, D. Tang, D. Knopp, CRISPR-cas12a-derived photoelectrochemical biosensor for point-of-care diagnosis of nucleic acid, Anal. Chem. 94 (2022) 7442–7448.
[43] X. Zhang, S. Liu, W. Zhang, X. Wang, L. Han, Y. Ling, N. Li, H. Luo, Photoelectrochemical platform for glucose sensing based on g-C_3N_4/$ZnIn_2S_4$ composites coupled with bi-enzyme cascade catalytic in-situ precipitation, Sens. Actuators, B 297 (2019), 126818.
[44] G. Chen, Y. Qin, L. Jiao, J. Huang, Y. Wu, L. Hu, W. Gu, D. Xu, C. Zhu, Nanozyme-activated synergistic amplification for ultrasensitive photoelectrochemical immunoassay, Anal. Chem. 93 (2021) 6881–6888.
[45] M. Cao, H. Wang, H. Tang, D. Zhao, Y. Li, Enzyme-encapsulated zeolitic imidazolate frameworks formed inside the single glass nanopore: catalytic performance and sensing application, Anal. Chem. 93 (2021) 12257–12264.
[46] L. Zhu, Z. Lv, Z. Yin, D. Tang, Double ion-exchange reaction-based photoelectrochemical immunoassay for sensitive detection of prostate-specific antigen, Anal. Chim. Acta 1149 (2021), 338215.